tumor mass rather than the cytotoxicity induced by an ADCC mechanism (*25*). We conclude that the targeting of human LAK cells to colon tumors is an important factor in the inhibition of tumor growth in vivo and that the SCID mouse–human xenogeneic chimeric model is useful for the study of anti-tumor properties of human effector cells. As demonstrated by the results of the present studies, it will be possible to test genetically modified human effector cells by conjugating the cells with tumor-specific antibodies to further increase their anti-tumor effects (*26*).

REFERENCES AND NOTES

1. E. A. Grimm, A. Mazumder, H. Z. Zhang, S. A. Rosenberg, *J. Exp. Med.* **155**, 1823 (1982); J. H. Phillips and L. L. Lanier, *ibid.* **164**, 814 (1986).
2. S. A. Rosenberg *et al.*, *N. Engl. J. Med.* **313**, 1485 (1985); W. H. West *et al.*, *ibid.* **316**, 898 (1987).
3. I. Kawase *et al.*, *Cancer Res.* **48**, 1173 (1988).
4. B. Mukherji *et al.*, *Int. J. Radiat. Appl. Instrum. B* **15**, 419 (1988).
5. G. C. Bosma, R. P. Custer, M. J. Bosma, *Nature* **301**, 527 (1983); M. J. Bosma and A. M. Carroll, *Annu. Rev. Immunol.* **9**, 323 (1991).
6. D. E. Mosier, R. J. Gulizia, S. M. Baird, D. B. Wilson, *Nature* **335**, 256 (1988); J. M. McCune *et al.*, *Science* **241**, 1632 (1988); R. B. Bankert *et al.*, *Curr. Top. Microbiol. Immunol.* **152**, 201 (1989); K. Pfeffer, K. Heeg, R. Bubeck, P. Conradt, H. Wagner, *ibid.*, p. 212; E. Simpson, J. Farrant, P. Chandler, *Immunol. Rev.* **124**, 97 (1991).
7. I. G. H. Schmidt-Wolf, R. S. Negrin, H.-P. Kiem, K. G. Blume, I. L. Weissman, *J. Exp. Med.* **174**, 139 (1991).
8. H. Takahashi *et al.*, *Gastroenterology* **96**, 1317 (1989).
9. The SCID–human colon cancer model was established according to the method described in (*8*), with modification. SCID mice anesthetized by intraperitoneal injection of 2% chloral hydrate (0.4 ml per mouse) were injected with 10^6 LS 180 cells and 20 μg of rabbit antibodies to asialo G_{M1} (Wako) in 0.25 ml of PBS (injection into the portal vein via splenic hilus with a 27-gauge needle). After 1 min, the portal vein was ligated and the spleen removed.
10. I. J. Fidler, *Cancer Res.* **50**, 6130 (1990).
11. H. Nelson, *Cancer Cells* **3**, 163 (1991).
12. B. Wilson *et al.*, *Proc. Natl. Acad. Sci. U.S.A.* **85**, 3140 (1988); H. Takahashi *et al.*, *Cancer Res.* **48**, 6573 (1988).
13. H. Takahashi, unpublished data.
14. K. Dorshkind, S. B. Pollack, M. J. Bosma, R. A. Phillips, *J. Immunol.* **134**, 3798 (1985); G. J. Bancroft, R. D. Schreiber, E. R. Unanue, *Immunol. Rev.* **124**, 5 (1991).
15. D. Herlyn and H. Koprowski, *Proc. Natl. Acad. Sci. U.S.A.* **79**, 4761 (1982); Z. Steplewski *et al.*, *ibid.* **85**, 4852 (1988); W. J. Johnson *et al.*, *J. Immunol.* **136**, 4704 (1986).
16. J. F. Jones and D. M. Segal, *J. Immunol.* **125**, 926 (1980).
17. MAb c-SF-25 was produced and provided by Centocor Inc. (Malvern, PA). We constructed a human-mouse chimeric Ig gene by joining variable region genes of light and heavy chains isolated from MAb SF-25 hybridoma cells to constant region genes of human κ light and γ 1 heavy chains. This construct was then transfected into Sp2/0 myeloma cells to produce the chimeric MAb.
18. J. R. Ortaldo, A. Mason, R. Overton, *J. Exp. Med.* **164**, 1193 (1986); K. Roberts, M. T. Lotze, S. A. Rosenberg, *Cancer Res.* **47**, 4366 (1987).
19. J. C. Unkeless, *J. Clin. Invest.* **83**, 355 (1989); J. V. Ravetch and J. P. Kinet, *Annu. Rev. Immunol.* **9**, 457 (1991).
20. LAK cells were incubated with MAb c-SF-25 (2 mg/ml) in RPMI 1640 for 30 min at 4°C. An equal volume of 30% PEG 8000 (Sigma) in RPMI 1640 was added to this cell mixture and incubated for an additional 90 min at 4°C. Finally, the cells were washed with PBS three times. As a control, human LAK cells were incubated with MAb c-SF-25 (2 mg/ml) for 90 min at 4°C and washed three times.
21. E. Vivier *et al.*, *J. Immunol.* **146**, 206 (1991).
22. S. A. Rosenberg *et al.*, *N. Engl. J. Med.* **319**, 1676 (1988).
23. J. T. Kurnick, R. L. Kradin, R. Blumberg, E. E. Schneeberger, L. A. Boyle, *Clin. Immunol. Immunopathol.* **38**, 357 (1986); L. M. Muul, P. J. Spiess, E. P. Director, S. A. Rosenberg, *J. Immunol.* **138**, 989 (1987).
24. B. Fisher *et al.*, *J. Clin. Oncol.* **7**, 250 (1989); K. D. Griffith *et al.*, *J. Natl. Cancer Inst.* **81**, 1709 (1989).
25. R. J. Dearman *et al.*, *Blood* **72**, 1985 (1988); A. W. Tong, J. C. Lee, R.-M. Wang, G. Ordonez, M. J. Stone, *Cancer Res.* **49**, 4103 (1989).
26. K. Nishihara *et al.*, *Cancer Res.* **48**, 4730 (1988); S. A. Rosenberg *et al.*, *N. Engl. J. Med.* **323**, 570 (1990); T. Friedmann, *Cancer Cells* **3**, 271 (1991).

27. Supported by grants CA-57584 and CA-35711 from the National Institutes of Health. We thank J. R. Wands and K. J. Isselbacher for review of the manuscript and for advice and support and R. Carlson and M. Nakaki for assistance.

2 October 1992; accepted 17 December 1992

Optical Time-of-Flight and Absorbance Imaging of Biologic Media

David A. Benaron and David K. Stevenson

Imaging the interior of living bodies with light may assist in the diagnosis and treatment of a number of clinical problems, which include the early detection of tumors and hypoxic cerebral injury. An existing picosecond time-of-flight and absorbance (TOFA) optical system has been used to image a model biologic system and a rat. Model measurements confirmed TOFA principles in systems with a high degree of photon scattering; rat images, which were constructed from the variable time delays experienced by a fixed fraction of early-arriving transmitted photons, revealed identifiable internal structure. A combination of light-based quantitative measurement and TOFA localization may have applications in continuous, noninvasive monitoring for structural imaging and spatial chemometric analysis in humans.

The principles that underlie the imaging of the interior of living bodies with light have application to a variety of situations that involve radiation transmission through opaque scattering media. Images can be formed with x-ray tomography (*1*), magnetic resonance (*2*), ultrasound (*3*), positron emission (*4*), thermal emission (*5*), electrical impedance (*6*), and other probes; but these have drawbacks that limit their use in the continuous, noninvasive monitoring of humans (*7*). Light, on the other hand, is nonionizing, relatively safe, and known to function well as a medical probe (*8–13*). In particular, red and near-infrared light pass easily through structures such as the skull (*9*), penetrate deeply into many tissues (*10*), are well tolerated in large doses (*11*), and can be used to quantitate chemical concentrations if an optical path length is known or estimated (*12*).

Variations in tissue absorbance and scattering over space and time influence photon travel through tissue. For example, breast tumors often attenuate light to a greater degree than neighboring tissues, possibly because of the presence of numerous blood vessels and mitochondria (*11, 13*). Spatial variations in absorbance have been used to form transillumination "shadowgrams" of such tumors (*13*), to detect cerebral bleeding (*14*), and to reconstruct two-dimensional steady-state tomographs (*15*). Temporal variations in absorbance, which can be caused by optical changes in certain proteins as oxygen pressure varies (*16*), have been used to estimate changes in the oxygenation of the brain (*8, 12, 17*) and extremities (*18*) and to measure blood flow and volume in tissues (*19*). Spectral analysis may also permit in vivo quantitation of substances such as glucose and cholesterol (*20*).

Optical imaging (*7*) and spectroscopy (*20*) in vivo have been difficult. With conventional radiological methods, photon scattering is minimal and, therefore, radiation travel is linear. In contrast, light takes highly irregular, diffusive paths through tissue, degrading image quality; detail is lost much as it is with distance in a fog. Scattering is the major attenuator of the intensity of transmitted photons in tissue (*21*). On average, a photon travels only millimeters into tissue, or less, before it scatters (*22*). Multiple scattering events occur for virtually all photons that propagate through tissue (*22, 23*), which causes them to take a wide range of paths as they traverse the tissue, each requiring a different amount of time. Because path lengths vary with absorbance and scattering, they are difficult to predict (*12*).

Medical Spectroscopy and Imaging Laboratory Section, Neonatal and Developmental Biology Laboratory, Department of Pediatrics, Stanford University School of Medicine, Palo Alto, CA 94305.

Time-resolved methods for optical tissue imaging, which were first suggested in 1971 (*24*), generally fall into two categories: (i) all photons are imaged, and an image is mathematically reconstructed from delays that are experienced by a group of photons as they travel from the emitter to the detector, or (ii) an image is formed with the use of only those photons that pass through tissue without scattering, which means that the photon path is linear and conventional radiological analysis is applicable. The former approach has yielded images for both real and ideal data but is computation-intensive and slow (*25*); on the other hand, the rarity of unscattered "ballistic" photons in tissue makes the latter approach possible only through collection of the more common minimally scattering "snake-like" photons (*26*). Optical variation along the emitter-detector axis disproportionately affects the transmitted intensity and transit times of ballistic and snake photons. Photon intensity has been integrated over fixed time windows early in the collection to image phantom objects through chicken breast several millimeters thick and other media (*26, 27*), to collect light through portions of a fish body (*28*), and to improve optical localization of the bones in fingers (*29*). However, imaging of an intact animal body had not yet been clearly shown.

Because freedom in the path of a photon increases with transit time, the contribution of each subsequently detected photon to image resolution is diminished. Therefore, image quality may be improved by maximizing collection of these spatially informational early photons. We suggested that, instead of using a fixed-interval time window, which collects a different proportion of the earliest photons whenever their time of arrival varies, it would be advantageous to use a variable-interval time window to collect photons until a fixed percentage of the total transmitted photons have been received. Such an approach detects a constant fraction of early photons, regardless of their transit times. The time required for the collection of this specified fraction of the total transmitted light, termed the "threshold time," serves as an imaging variable.

To test this approach, we developed a portable TOFA system that records a transit time for each photon that is detected (*7*). The system, modified from a commercial optical time-domain reflectometer (Opto-electronics, Ontario, Canada), consists of up to three diode lasers that are coupled by fiber optics to the base of an automated translational stage, on which the objects to be imaged are placed (Fig. 1). Images are generated during a two-dimensional scan by the accumulation of one TOFA curve at each (X,Y) stage location. As each measured threshold time primarily reflects the optical properties of tissue that lies on a line directly between the emitter and detector, only one TOFA curve is required to calculate the value of each image pixel, with a measurement from each stage location corresponding to a single pixel in the final image. About 30 s is required for measurement and analysis of each pixel (*30*). The resolution of the mean path length for an unscattered pulse in water is better than 500 μm. Changes in threshold times are calculated for each pixel as compared with an appropriate reference. Analysis of a constant fraction of the early photons with this TOFA device resulted in simplified calculations and the successful imaging of phantoms (*7*). We then tested if TOFA imaging could be successful in biologic systems.

Two experiments were performed. First, to demonstrate that variable-window TOFA imaging applies to media that scatter photons to the same degree as biologic tissues, we collected data at one central location through four tissue models. The models were thin-walled 700-cm^3 cubes of opaque acrylic, similar in volume to the head of a premature neonate, each filled with a dilute soybean-based lipid emulsion (20% intravenous fat emulsion, Baxter-Travenol Laboratories, Roundlake, Illinois) known to scatter light similarly to human tissue. The four models contained (i) lipid alone, (ii) lipid with a centrally placed black matte rod that blocked light, (iii) lipid with rods placed on either side of the emitter-detector axis, and (iv) lipid with centrally placed human tissue (fingers). The emitter and detector were separated by 90 mm, the width of the detection window was 5 ns, and the wavelengths that we analyzed were 780 and 850 nm. Time-of-flight curves were plotted and threshold times of 1% were calculated as compared with a reference of lipid alone.

For the second experiment, data were collected at multiple locations over a 30 by 16 grid from a dead 10-day-old rat pup that was suspended in blood and placed on the translational stage. The emitter and detector were separated by 35 mm, which is equal to the depth of blood needed to submerge the animal, the image area was 75 by 40 mm, the width of the detection window was 4 ns, and the wavelength that we analyzed was 904 nm. The relative photon intensity was calculated and stored in a 30 by 16 matrix at a location that corresponded to the stage coordinate of that measurement. The matrix pixels were then assigned false colors with the use of a logarithmic magnitude scale and were imaged on film. Similarly, the change in threshold delay for each pixel was calculated relative to the threshold time for light passing through blood alone, was reduced by 25 ps to provide a margin for background

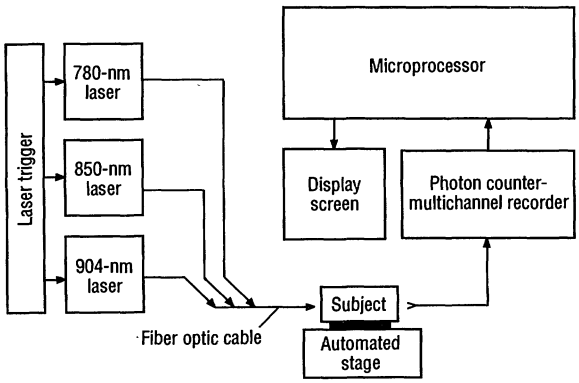

Fig. 1. A time-of-flight and absorbance (TOFA) optical system. Light from up to three lasers is temporally separated, fed into a single fiber optic cable, and directed to the base of an automated positioning stage. Transmitted light is collimated by a detector fiber and passed to a time-gated multichannel photon counter, which accumulates and averages multiple curves. Results are stored until a grid of data is collected and are then displayed on a color monitor.

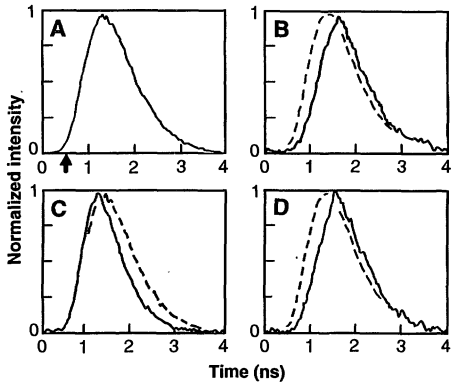

Fig. 2. Normalized TOFA curves through four tissue models. Scattering during transmission through lipid alone (**A**) yields a wide time-intensity curve (shown dashed in remaining figures). Threshold time (T), the time of arrival of first 1% of total transmitted light, is indicated by arrow. Blocking the direct optical path with rods (**B**) or finger (**D**) results in loss of earliest arriving signals and delay in threshold time (ΔT = 139 and 163 ps, respectively) as compared to a reference threshold time through lipid alone in (A). Blocking the peripheral optical path (**C**) results in loss of later arriving signals but does not appreciably alter threshold time (ΔT = 16 ps). Curves collected at 780 nm; results at 850 nm were similar. Time zero (414 ps) and absorbance [A = log (photon attenuation)] were based on unscattered transmission through water. Absorbance and mean path length were, respectively, (A) = 5.1, 362 mm; (B) 6.3, 409 mm; (C) 5.5, 316 mm; and (D) 6.2, 405 mm.

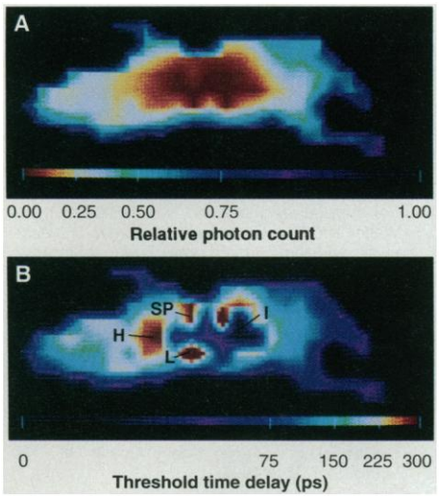

Fig. 3. Scan of a rat with the use of TOFA imaging. An image of steady-state photon transmission (**A**) is unrevealing, whereas a time-resolved TOFA image of threshold times (**B**), which was generated from time-of-flight curves at each image coordinate, reveals internal structure. Intestinal gas is visible as a decreased threshold in the abdomen. H, heart; L, liver; I, intestines; SP, spleen and pancreas.

noise, and was placed in a similar matrix. That matrix was assigned false colors on the basis of the magnitude of change in threshold delay and was imaged on film. After data collection, x-ray films of the rat were obtained, and an autopsy was performed to document the actual organ location. Animals were handled in accordance with university regulations.

Through lipid alone (Fig. 2A), photon attenuation exceeded 10^5, as compared with transmission through water alone. A ratio of scattered to unscattered mean path length was 4.09, which is similar to the lengthening produced by scattering in neonatal brain (*12*). Obstruction of the line-of-sight photon paths blocked the minimally scattering photons, which diminished the initial portion of the TOFA curve (Fig. 2B); obstruction of off-center paths blocked highly scattering photons, which diminished the terminal portion of the curve (Fig. 2C); a human finger absorbed photons, in addition to scattering them, which diminished the early portion of the curve (Fig. 2D). The presence of absorptive or scattering objects on the emitter-detector axis increases threshold time more than objects outside the direct path, which supports the view that the photons that are detected first are likely to have spent the majority of time traveling in a narrow central region directly between the emitter and detector, whereas the photons that are detected later are likely to have diverged well into the medium.

It took 4 hours to scan the rat and 15 min to process and film the image. Maximum photon attenuation was not calibrated but was estimated to be 10^8. An image of the steady-state distribution of absorbance over space is unrevealing; it only shows greater absorbance in thicker portions of the body (Fig. 3A). On the other hand, a time-resolved image of threshold times reveals major features: heart, liver, spleen and pancreas, and intestinal gas (Fig. 3B). The locations correlate with x-ray and autopsy results.

Our results show that TOFA methods allow the imaging of scattering media such as intact animals, which is an advantage of path-sensitive over absorbance-sensitive approaches to tissue imaging. Both time- and frequency-resolved techniques have been shown to be useful path-sensitive approaches to image reconstruction and subsurface object detection, and both approaches yield theoretically equivalent data that are related by a Fourier transform (*31*). In the frequency domain, Chance *et al.* (*14*) pioneered multifrequency amplitude-modulated phase shift spectrophotometry in which phase shifts, which are related to the average delays experienced by photons traveling through tissue, are measured as a function of modulation frequency. Sevick and co-workers (*32*) have shown that such a variable-frequency approach, when used in the reflection geometry needed to image tissues too thick for transillumination, gives the investigator control over depth of focus and is the frequency-domain equivalent of variable-interval time windows. Chance (*33*) and Fishkin *et al.* (*34*) have been using phased arrays as a probe, an interesting variation that is similar to ultrasonography and radar. Other laboratories, besides ours, have focused on time-resolved approaches. With the use of images reconstructed mathematically from time-of-flight curves taken at multiple locations, Arridge *et al.* (*35*) have demonstrated three-point structure resolution, which reduces computation time to 20 min under carefully controlled initial conditions. There are also strong parallels with impedance imaging, which are now being explored. We favor a time-domain approach because path length is determined for each detected photon, as opposed to the ensemble averages that are determined by frequency-domain approaches. However, it remains unclear at this time which method will prove superior, and it is likely that each will have strong points that support use under certain clinical conditions.

Several points concerning our data are important. First, resolution in vivo may be superior to that obtained in our lipid model because the high concentrations of absorbers in vivo should substantially decrease the number of pulse-widening, highly scattered photons (*7, 29*). Second, our device exhibits resolution superior to what would be expected given the width of the laser pulse. This may be attributable to our use of only the first fraction of the detected photons, which would narrow the effective laser pulse considerably at the cost of decreasing the effective photon intensity. Also, by averaging multiple laser pulses, we achieved a reduction in noise. We currently estimate the limits of detection to be at 5 mm in neonatal brain and 2 mm in the adult breast. Third, the animal's lungs are not well visualized, which could be attributable to postmortem lung collapse and to the submersion of the rat in blood during imaging, which was done to minimize boundary anomalies caused by mismatching of scattering, absorbance, and refractive indices. Finally, the equipment and computations that we have used to generate these images are unlikely to be optimal. Specific improvements, such as additional collimation of the detected light signal, higher repetition rates, detector arrays, and higher powered diode lasers (still portable and well within the limits of human safety), could easily decrease the imaging time by a factor of 10^5 or more.

It is likely that there are several clinical conditions that could benefit from such optical devices, even in the absence of further technological breakthroughs. Optical imaging may allow continuous in vivo imaging, and combination with spectroscopy may allow chemical analysis, such as glucose measurement. By providing a distribution of photon path lengths, TOFA imaging may make possible quantitative optical measurement of deep-tissue oxygenation, which was first proposed by Jöbsis (*8*), as well as localization of that measurement. Current tools for the evaluation of neurologic function are inadequate for the early detection of brain injury that is caused by a lack of oxygen, and therefore identification of the nature and timing of these injuries is likely to lead to health-saving and life-saving intervention. Light-based imaging may also permit diffusometry (*33*), the characterization of tissue and tissue components based on optical properties, which would allow remote pathological typing of tumors and other tissues. Lastly, spectral discrimination may lead to remote identification of tissue by type—of fresh blood clot from old or of frozen tissue from untreated in tumors undergoing cryotherapy—or even detailed chemometric analysis.

An advantage of our approach is the simplicity of the calculations: each pixel is independent of neighboring ones, which allows for on-the-fly computation. The development of clinically relevant model systems will allow comparison between, and standardization of, different optical imaging techniques, while progress in the development of new optical tools may result in the

construction of affordable, portable optical imaging systems.

REFERENCES AND NOTES

1. G. N. Hounsfield, *Br. J. Radiol.* **46**, 1016 (1973).
2. R. Damadian, M. Goldsmith, L. Minkoff, *Physiol. Chem. Phys.* **9**, 97 (1977).
3. J. J. Wild and J. M. Reid, *Science* **115**, 226 (1952).
4. G. D. Hutchins *et al.*, *IEEE Trans. Nucl. Sci.* **NS32**, 835 (1985).
5. A. M. Gorbach and E. N. Tsicalov, *Proc. IEEE Eng. Med. Biol. Soc.* **12**, 1245 (1990).
6. J. C. Newlee, D. G. Gisser, D. Isaacson, *IEEE Trans. Biomed. Eng.* **35**, 828 (1988).
7. D. A. Benaron, M. A. Lenox, D. K. Stevenson, *SPIE* **1641**, 35 (1992).
8. F. F. Jöbsis, *Science* **198**, 1264 (1977).
9. P. W. McCormick, M. Stewart, G. Lewis, M. Dujovny, J. I. Ausman, *J. Neurosurg.* **76**, 315 (1992); C. D. Kurth, J. M. Steven, D. A. Benaron, B. Chance, *J. Clin. Monit.*, in press.
10. B. Chance *et al.*, *Proc. Natl. Acad. Sci. U.S.A.* **85**, 4971 (1988); D. T. Delpy *et al.*, *Phys. Med. Biol.* **33**, 1433 (1988); L. O. Svaasand and R. Ellingsen, *J. Cereb. Blood Flow Metab.* **3**, 293 (1983).
11. J. C. Hebden and R. A. Kruger, *Med. Phys.* **17**, 41 (1990).
12. J. S. Wyatt *et al.*, *Dev. Neurosci.* **12**, 140 (1990); D. A. Benaron *et al.*, *IEEE Eng. Med. Biol. Mag.* **12**, 2004 (1990); D. A. Benaron *et al.*, *ibid.*, p. 1117 (1990); H. Mark, *Anal. Chim. Acta* **223**, 75 (1989).
13. B. Drexler, J. L. Davis, G. Schofield, *Radiology* **157**, 41 (1985); V. Marshall, D. C. Williams, K. D. Smith, *ibid.* **150**, 339 (1984); G. Navarro and A. Profio, *Med. Phys.* **15**, 181 (1988).
14. B. Chance, *SPIE* **1641**, 162 (1992).
15. J. R. Singer, F. A. Grünbaum, P. Kohn, J. P. Zubelli, *Science* **248**, 990 (1990); R. Araki and I. Nàshimoto, *SPIE* **1431**, 321 (1991).
16. These proteins include hemoglobin, myoglobin, mitochondrial cytochrome aa_3, cytosolic cytochrome oxidase, and other copper- or iron-containing proteins.
17. P. W. McCormick *et al.*, *Crit. Care Med.* **19**, 89 (1991); J. E. Brazy, D. V. Lewis, M. G. Mitnick, F. F. Jöbsis, *Adv. Exp. Med. Biol.* **191**, 843 (1986).
18. M. Ferrari, Q. Wei, L. Carraresi, R. A. DeBlasi, G. Zaccanti, *J. Photochem. Photobiol.*, in press; C. M. Alexander, L. E. Teller, J. B. Gross, *Anesth. Analg. (Cleveland)* **68**, 368 (1989); G. A. Millikan, *Rev. Sci. Instrum.* **4**, 434 (1942); D. A. Benaron, W. E. Benitz, R. A. Ariagno, D. K. Stevenson, *Clin. Pediatr. (Philadelphia)* **31**, 258 (1992).
19. J. S. Wyatt, A. D. Edwards, D. Azzopardi, E. O. Reynolds, *Arch. Dis. Child.* **64**, 953 (1989); J. S. Wyatt *et al.*, *J. Appl. Physiol.* **68**, 1086 (1990); A. D. Edwards *et al.*, *Lancet* **335**, 1491 (1990).
20. I. Amato, *Science* **258**, 892 (1992).
21. B. C. Wilson, M. S. Patterson, S. T. Flock, D. R. Wyman, in *Photon Migration in Tissues*, B. Chance, Ed. (Plenum, New York, 1990), p. 29.
22. S. T. Flock, B. C. Wilson, M. S. Patterson, *Med. Phys.* **14**, 835 (1987).
23. M. S. Patterson, B. Chance, B. C. Wilson, *Appl. Opt.* **28**, 2331 (1989); K. M. Yoo and R. R. Alfano, *Opt. Lett.* **15**, 320 (1990).
24. M. A. Duguay and A. T. Mattick, *Appl. Opt.* **10**, 2162 (1971).
25. F. H. Schlereth, J. A. Fossaceca, A. D. Keckler, R. L. Barbour, *SPIE* **1641**, 46 (1992); R. L. Barbour *et al.*, *ibid.*, p. 21.
26. L. Wang, P. P. Ho, C. Liu, G. Zhang, R. R. Alfano, *Science* **253**, 769 (1991).
27. J. C. Hebden, R. A. Kruger, K. S. Wong, *Appl. Opt.* **30**, 788 (1991); K. M. Yoo, F. Liu, R. R. Alfano, *Opt. Lett.* **16**, 1068 (1991).
28. L. Wang, Y. Liu, P. P. Ho, R. R. Alfano, *SPIE* **1431**, 97 (1991).
29. S. Andersson-Engels, R. Berg, S. Svanberg, *Opt. Lett.* **15**, 1179 (1990).
30. Beam diameter was 50 μm, temporal half-maximum width was 100 ps, peak power ranged from 10 mW at 780 nm to 50 mW at 904 nm, repetition rate was 33 kHz, and triggering was reproducible to within 2 ps. Lasers fire simultaneously, whereas differences in fiber length temporally separated the signals. A detector fiber, 50 μm in diameter and located such that linear photon collection was maximized, collimated, and transmitted detected light to a solid-state photon counter with up to 25% efficiency. The laser was triggered 256 times to collect a single curve as the detector was sampled, once each pulse, over a series of sequential, partially overlapping detection windows. Results were accumulated in a multichannel recorder. Minimum transit-time increment between adjacent sampling windows was 2 ps. Multiple curves were accumulated and averaged per pixel. The translational stage was computer-controlled in 500-μm steps over two axes. A reference pulse through air, water, or blood, as appropriate, was used to determine time zero.
31. J. R. Lakowicz, G. Laczko, H. Cherek, E. Gratton, M. Limkeman, *Biophys. J.* **46**, 463 (1984); S. R. Arridge, M. Cope, D. T. Delpy, *Phys. Med. Biol.* **37**, 1531 (1992).
32. E. M. Sevick, J. R. Lackowicz, H. Szmacinski, K. Nowaczyk, M. L. Johnson, *J. Photochem. Photobiol.*, in press; E. M. Sevick, in *Oxygen Transport to Tissue XV*, P. Vaupel, Ed. (Plenum, New York, in press).
33. B. Chance, in *Oxygen Transport to Tissue XV*, P. Vaupel, Ed. (Plenum, New York, in press).
34. F. Fishkin, E. Gratton, M. J. vandeVen, W. W. Mantulin, *SPIE* **1431**, 123 (1991); A. Knüttel, J. M. Schmitt, J. R. Knutsen, *Appl. Opt.*, in press.
35. S. R. Arridge, P. van der Zee, M. Cope, D. T. Delpy, *SPIE* **1431**, 204 (1991).

36. For support we thank the NIH (RR-00081), the Walter and Idun Berry Fund for Human Development, and the Zaricor Family Fund at Stanford; for assistance we thank M. A. Lenox, M. Goheen, and D. Ho. Preliminary studies, on which this report was based, were presented at the "Progress in Biomedical Optics" Meeting, Biomedical Optics Society (BiOS) and the Society of Photo-Optical Instrumentation Engineers (SPIE), Los Angeles, 22 to 23 January 1992, and at the NIH Workshop on Near-Infrared Spectroscopy, D. Hirtz, chair, National Institute of Neurological Diseases and Stroke, Chevy Chase, MD, 30 March to 1 April 1992.

22 January 1992; accepted 15 December 1992

Requirement for a GTPase-Activating Protein in Vesicle Budding from the Endoplasmic Reticulum

Tohru Yoshihisa, Charles Barlowe, Randy Schekman

The binding and hydrolysis of guanosine triphosphate (GTP) by the small GTP-binding protein Sar1p is required to form transport vesicles from the endoplasmic reticulum (ER) in *Saccharomyces cerevisiae*. Experiments revealed that an interaction between Sar1p and the Sec23p subunit of an oligomeric protein is also required for vesicle budding. The isolated Sec23p subunit and the oligomeric complex stimulated guanosine triphosphatase (GTPase) activity of Sar1p 10- to 15-fold but did not activate two other small GTP-binding proteins involved in vesicle traffic (Ypt1p and ARF). Activation of GTPase was inhibited by an antibody to Sec23p but not by an antibody that inhibits the budding activity of the other subunit of the Sec23p complex. Also, activation was thermolabile in pure samples of Sec23p that were isolated from two independent *sec23* mutant strains. It appears that Sec23p represents a new class of GTPase-activating protein because its sequence shows no similarity to any known member of this family.

Protein transport between membrane-bound organelles is mediated by cytosolic and membrane proteins that facilitate the formation, targeting, and fusion of small carrier vesicles (*1*, *2*). An interacting set of *SEC* genes contribute to vesicle budding early in the secretory pathway of *S. cerevisiae* (*3*). Two of these Sec proteins have been purified by means of an assay that reproduces the vesicle-budding event in vitro (*4*–*7*). The first protein, Sar1p, is a small GTP-binding protein that is representative of a large class of proteins similar to Ras that are associated with intracellular membrane traffic (*8*–*10*). The second, Sec23p, is part of a hetero-oligomeric complex, both subunits of which are required for vesicle budding in vitro (6). A mammalian homolog of Sec23p has been immunolocalized to the vesicles, cytoplasm, and tubular extensions of the ER transitional zone adjacent to the Golgi apparatus (*11*).

We isolated two functional forms of Sec23p by biochemical complementation of a *sec23* mutant lysate in an assay of ER-to-Golgi transport. Extracts of cells in which *SEC23* is overexpressed yielded an active monomeric species and the hetero-oligomeric Sec23p complex, whereas extracts of wild-type cells yielded only the complex (6). In an effort to identify other factors that interact with Sec23p, we examined the effect of excess monomer and complex on transport vesicle formation in a wild-type lysate. Briefly, the vesicle budding reaction measures the transfer of a radioactive secretory glycoprotein, yeast α-factor precursor, from rapidly sedimenting ER membranes to slowly sedimenting transport vesicles (*4*). The amount of Sec23p in a wild-type lysate was sufficient for vesicle formation. However, addition of excess Sec23p monomer inhibited budding (Fig. 1A) (*12*) whereas

Howard Hughes Medical Institute, Department of Molecular and Cell Biology, Barker Hall, University of California, Berkeley, CA 94720.